A. A NOVEL TWO-QUADRANT SOFT-SWITCHING CONVERTER WITH ONE AUXILIARY SWITCH FOR HIGH POWER APPLICATIONS

A-I. INTRODUCTION

There has been an increasing interest in the soft-switching power conversion technologies in order to overcome the limitations of the hard-switching technologies [1]-[7]. Soft-switching (SS) converters had many advantages over hard-switching (HS) converters. For example, SS converters lower switching losses, reduce voltage/current stress, reduce EMI, and allow a greater high switching frequency in high power applications [1]. Despite the advantages of SS converters, its applications have been so far limited due to complexity in the design of SS circuits, and difficult in control realization. There has been a growing demand for a simple design that provides reliable control in a wide-range of operational condition.

Several SS techniques have been developed such as the auxiliary resonant snubber inverter (RSI) [1], the auxiliary resonant commutated pole inverter (ARCP) [3], [6], the inductor coupled zero-voltage transition inverter (ZVT) [4]-[5], and the resonant dc link inverter (RDCL) [2], [7]. The RSI is suitable for single or three-phase inverters with multiple branches of auxiliary circuits but needs modification of space vector modulation to ensure zero voltage switching. The ARCP requires large split capacitors to achieve a zero-voltage switching. The ZVT requires bulky coupled inductors to reset the resonant current. The RDCL needs a device voltage rating higher than that which has been used in other converters.

This study found that the RSI can easily be extended to two-quadrant chopper applications, but it must use a variable boost current to meet different load current conditions. In a two-quadrant soft-switching (TQSS) converter, there are no switches available for current

boosting because it uses diodes in the current return path. Therefore, a new control-timing scheme is proposed in this TQSS converter with only one auxiliary branch to achieve near zero-voltage switching under all load-conditions.

In order to validate the proposed converter, computer simulations and experiments were conducted. In both the simulation and experiment, the purpose of the comparison between soft-switching and hard-switching was to investigate the following characteristics: the voltage spike, EMI noise, turn-off dv/dt, heat sink temperature, power loss and control flexibility. With the merits of simplicity and flexibility, the proposed TQSS converter shows excellent performance and potential for various industry applications including switched reluctance motor (SRM) drives, high-frequency-high-voltage choppers, magnet drivers, and magnetic resonance imaging (MRI) system applications.

A-II. PROPOSED CONVERTER TOPOLOGY AND ITS OPERATIONS

A. Operational Principles

Fig.A-1 shows the proposed two-quadrant soft-switching converter consisting of a pair of switches (S_1 and S_2), a pair of diodes (D_1 and D_2), and one auxiliary switch. The two switches are synchronously conducting or blocking depending on the desired switching duties. Two diodes provide a freewheeling current path and a reverse voltage across the load to form a two-quadrant operation. Notice that the load current is unidirectional. When the load current is flowing in diodes D_1 and D_2, turning on S_1 and S_2 would shut off the diode current, but on the other hand, produce a large diode reverse recovery current and turn-on loss. Snubber capacitors are added across the main devices to reduce turn off losses. The auxiliary branch is connected between the two phase-legs or across the load. This branch consists of one auxiliary switch, one fast recovery diode, and one resonant inductor. Fig. A-2 shows the key operating waveforms of the proposed converter circuit.

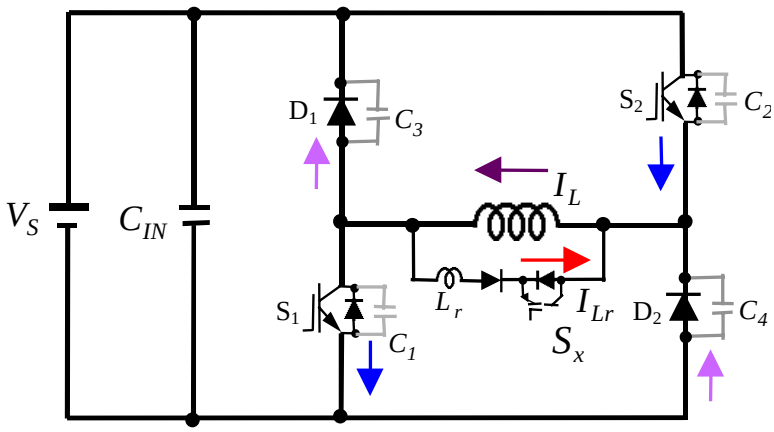

Fig. A-1. Proposed two-quadrant soft-switching converter.

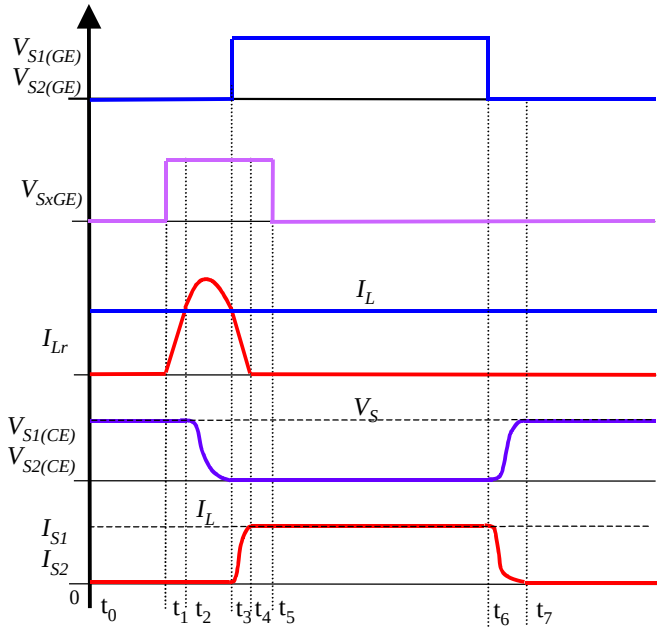

Fig. A-2. Operational waveforms of the proposed converter.

B. Circuit Analysis

For a simple circuit analysis, it is assumed that the load current remains constant during the one-cycle operation as shown in Fig. A-2. Under this assumption, analysis is performed on

the circuit for seven distinct operating modes in the period [t_0 - t_7]. Initially at time t_0, all the switches are off, and load current flows through D_1 and D_2.

Mode M0 ($t_0 - t_1$): Assuming that the load current is positive, the free-wheeling diodes D_1 and D_2 conduct the load current, and the main devices are off.

Mode M1 ($t_1 - t_2$): After the auxiliary switch, S_x, turns on, the inductor current, I_{Lr}, increases linearly until it equals the load current I_L. At this time, the current through D_1 and D_2 starts to decrease slowly to zero. The slope can be determined as a function of the resonant inductor and dc source as shown below.

$$\frac{di_{Lr}}{dt} = \frac{V_S - V_D}{L_r} \tag{A-1}$$

where V_D is the total conducting voltage across the switching devices. At time t_2, the resonant inductor current I_{Lr} equals the load current I_L and the diode currents reach zero. The charging time is calculated using

$$t_2 - t_1 = \frac{L_r \cdot I_L}{V_S} \tag{A-2}$$

In order to meet the energy balance requirement for the resonant components, the aforementioned energy requirement can be represented in (A3)

$$\frac{1}{2} L_r (I_{Lr} - I_L)^2 \geq C_r (V_S - V_D)^2 \tag{A-3}$$

where C_r is the equivalent resonant capacitance of the snubber capacitors, when C_1=C_2=C_3=C_4=C_r. This relationship indicates that the resonant capacitors, which are across the main devices, are either fully charged or discharged during resonance.

<u>Mode M2</u> ($t_2 - t_3$): The diodes, D_1 and D_2, are turned off naturally, when the resonant current is larger than the load current. The resonant capacitor and inductor resonate to discharge the capacitor voltage across the main switches. At time t_2, the initial device voltages, V_{S1} and V_{S2}, are equal to V_S. Fig. A-3 shows the equivalent circuit during **M2** mode, where the inductor is replaced by a current source, I_L. The initial value for the inductor current, I_{Lr}, is I_L, and for the resonant capacitor voltage, V_{Cr}, is V_S. Under these conditions, the resonant capacitor voltage and inductor current can be expressed as

$$V_{Cr}(t) = V_S \cdot (1 - cos(\omega t))$$

$$I_{Lr}(t) = I_L + \frac{V_S}{Z_r} \cdot sin(\omega t) \qquad \text{(A-4)}$$

where

$$\omega_r = \frac{1}{\sqrt{L_r \cdot C_r}}, Z_r = \sqrt{L_r / C_r} \qquad \text{(A-5)}$$

At time t_3, when the resonating cycle begins, V_{Cr} reaches zero and the parallel diodes of S_1 and S_2 provide a path for the resonant-current to control. The capacitor across the switch discharges at a finite rate allowing the switch voltage to drop to zero.

<u>Mode M3</u> ($t_3 - t_4$): By the end of the resonant period, t_3, the snubber capacitors are discharged to zero voltage. At this moment, the main switch can be turned on easily under zero-voltage condition. Without extravagant sensing, it is difficult to turn on the main switch at the exact moment the capacitor voltage drops to zero. Therefore, the main switch can only be turned on under a near-zero-voltage condition. When the main switches turn on, the inductor current decreases linearly due to reverse voltage polarity of the opposite diode.

<u>Mode M4</u> ($t_4 - t_5$): The resonant current decreases until it hits zero at t_4. The auxiliary switch and diode are then turned off under zero-current condition at t_5. The main switches now conduct the load current. The auxiliary switch and diode are both turned off after time t_4.

<u>Mode M5</u> (t_6 - t_7): After the steady-state, (t_5-t_6), the main switches turn off without loss using snubber capacitors, which carry the load current until diodes D_1 and D_2 turn on and the operation returns to **M0**.

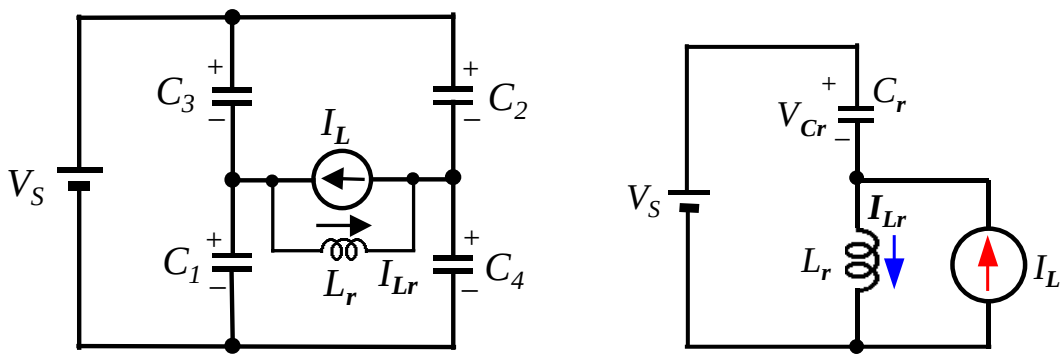

(a) Resonant stage circuit (b) Simplified equivalent circuit

Fig. A-3. Equivalent circuit during resonant mode.

A-III. CONVERTER CHARACTERISTICS

In This study, the proposed TQSS converter is characterized and modeled the converter's control flexibility by using Pspice circuit simulator, with commercial IGBT SPICE models.

A. Soft-Switching State-Plane Trajectory

In order to design the soft-switching circuit, the state plane trajectory diagram can be used widely. Fig. A-4 shows the key waveforms of the proposed converter when the dc bus voltage is 300-V and the load current is 25-A. It can be seen that the main switches operate well under near zero-voltage condition.

Fig. A-5 shows the state-plane trajectory for the same operating conditions. This diagram explains operational modes of the proposed converter. It is clear that the resonant tank impedance is independent of the load current condition as shown in (A-4). The peak value of the

resonant current is ($I_{Lr} - I_L$). As the load current increases the duration of the pre-charging modes M1 and discharging modes M3 increase.

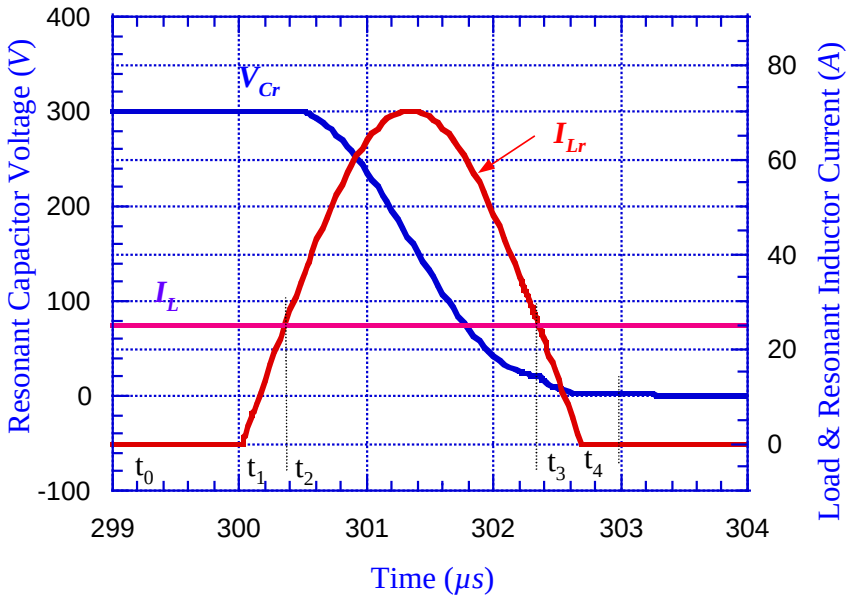

Fig. A-4. Simulated current and voltage waveforms of the converter under soft-switching.

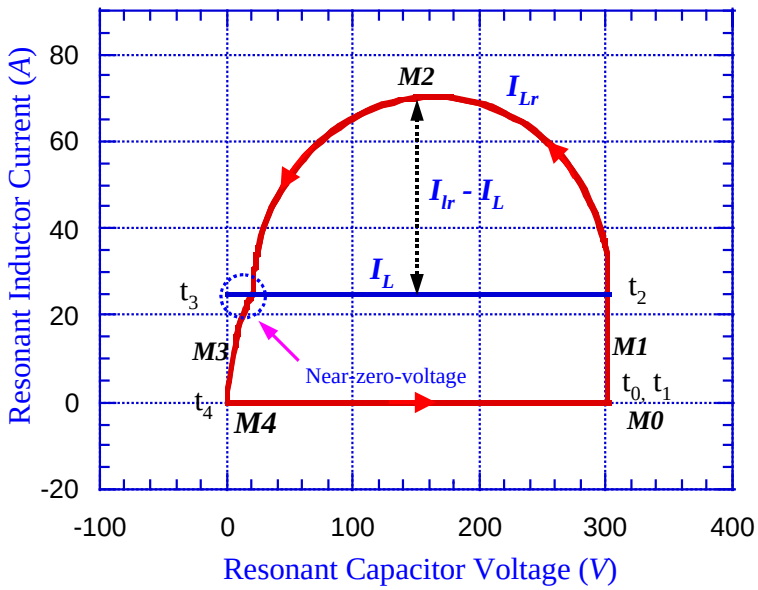

Fig. A-5. Soft-switching state-plane trajectory diagram.

The selection of the resonant capacitor is very crucial for proper operation of the circuit, because the resonant capacitor reduces the turn-off loss and turn-off dv/dt of the device. A larger size capacitor can reduce the turn-off loss and dv/dt. However, the extra energy stored in the resonant capacitor needs to be discharged during turn on. So, the capacitor size should be optimized so that both turn-on and turn-off losses are reduced. The rate of change of voltage across the resonant capacitor can be expressed as

$$\frac{dV_{CE}}{dt} = \frac{I_{sw}}{C_r} \tag{A-6}$$

where, V_{CE} is the collect-emitter voltage, and I_{sw} is the device current, which equals to the load current, I_L, during switching.

Fig. A-6 shows the measured turn-off energy under different snubber capacitors and load current conditions. As expected, it indicates that the turn-off switching energy is inverse-proportional to the resonant capacitor. The capacitance can be selected at the knee point where further increment of C_r not significantly reduces turn-off loss.

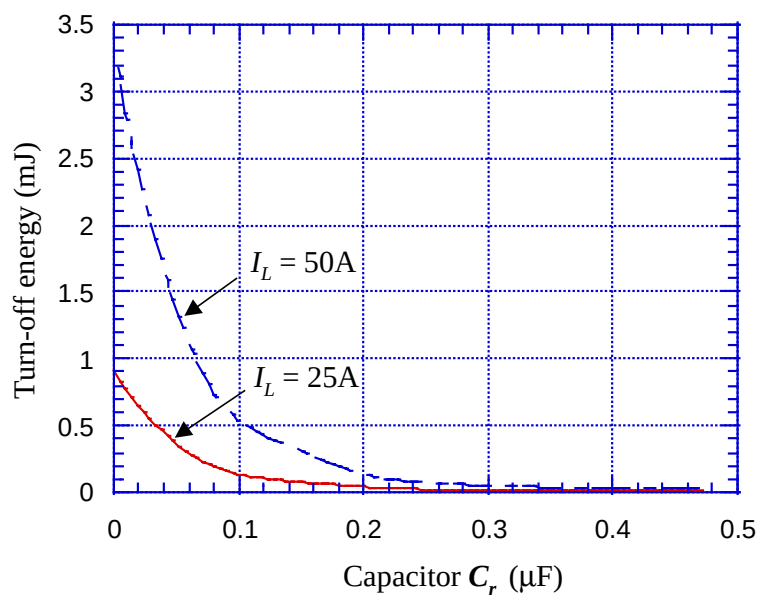

Fig. A-6. Turn-off energy vs. resonant capacitance under different load currents.

After selecting the resonant capacitor, the resonant inductor should be designed based on peak resonant current and the time to reach peak resonant current. These two factors can also be translated into the resonant tank impedance Z_r $(=\sqrt{L_r/C_r})$ and its resonant frequency f_r $(=1/2\pi\sqrt{L_rC_r})$. Using the values selected for the resonant capacitor and inductor, the auxiliary switch conduction time T_{aux} is as follows.

$$T_{aux} = 2 \cdot (L_r \cdot I_L)/V_S + \pi\sqrt{L_r C_r}\,) \qquad \text{(A-7)}$$

B. Control Flexibility

The proposed converter has a very flexible control scheme for wide variation in load current. This is because the resonant current follows the load current. Fig. A-7 indicates an example of an incorrect control scheme at the soft-switching instant. When the pre-turn-on time is longer than the design value, the main switch is turned on late and the switch voltage shows an irregularity during the time delay.

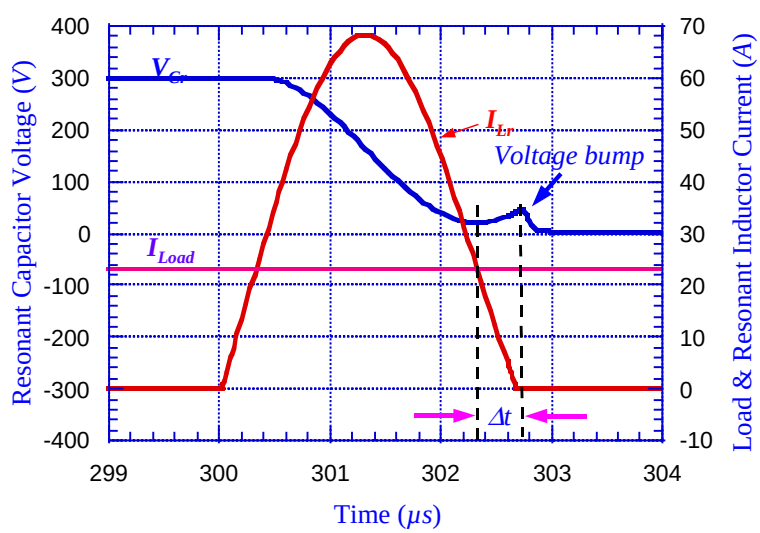

Fig. A-7. Resonant current and switch voltage waveforms under incorrect timing.

Figures A-8 (a) and (b) show the key soft-switching waveforms when the load currents are 11-A and 28-A, respectively. They show the timing diagrams for the voltage across the resonant capacitor, load current and the current in the resonant inductor. It can be seen that the main switches can achieve near zero-voltage turn-on condition under different load current conditions.

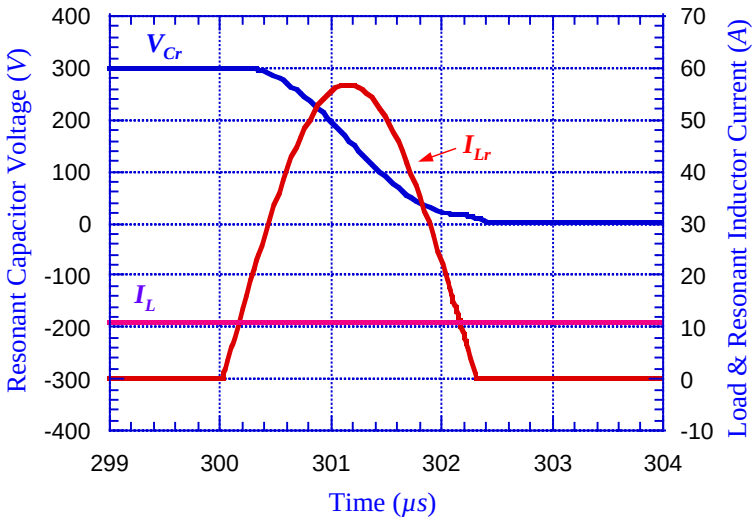

(a) Load current of 11-A

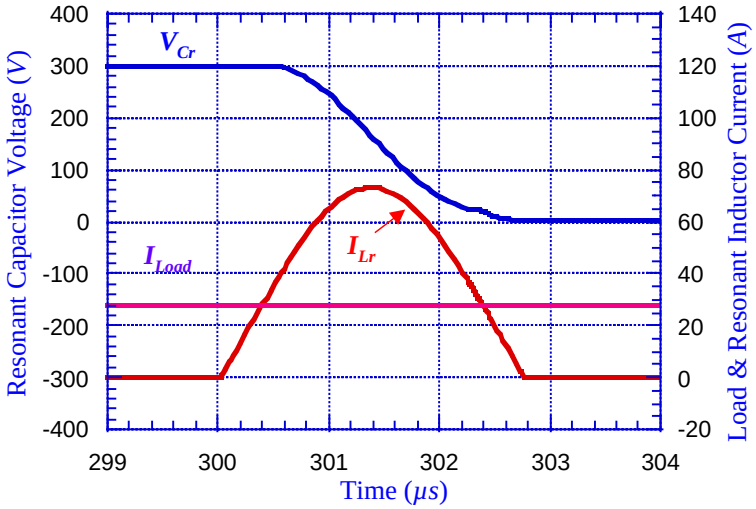

(b) Load current of 28-A

Fig. A-8. Waveforms of resonant current and switch voltage under different load current conditions.

Fig. A-9 shows the control block diagram of the converter and its gate signals for soft-switching operations. The gate signals for the S_1 and S_2 have a time delay of T_D, and the S_X signal has a fixed short pulse of T_{aux} generated by the PWM signal, whenever the rising edge on the PWM signals through the proportional-integrated (PI) current controller occurs. The parameters used in the experiment are explained as the following section.

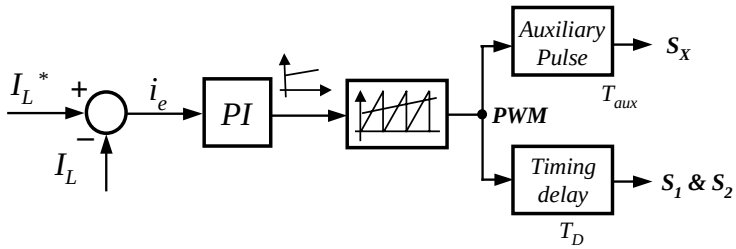

(a) Soft-switching control scheme

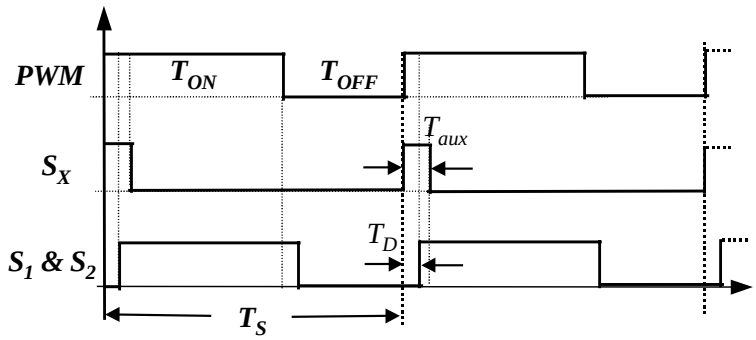

(b) Gate signals

Fig. A-9. Control block diagram under soft-switching.

A-4. EXPERIMENTAL RESULTS

In order to verify performance of the proposed converter, experiments were conducted using the value of the circuit parameters. These values are identical to those used for the simulation.

1) A dual IGBT module at 600V - 200A was used;

2) The resonant capacitors used were 0.1µF - 600V Polypropylene capacitors;
3) The resonant inductor used was 4.3 µH;
4) The auxiliary switch chosen was a 50A - 600V IGBT;
5) The blocking auxiliary diode was chosen as an HFA50PA60C rated at 50A - 600V; and
6) The auxiliary conducting time used was 3.5µs.

A. *Hard-Switching*

It is well known that the problems associated with hard-switching operations can be demonstrated by the IGBT device test. Fig. A-10 shows the IGBT switching voltage and current waveforms under hard-switching condition. It is seen that the switching characteristic of the IGBT used demonstrates a high turn-off dv/dt, a high voltage spike, and a large loss during turn-off conditions. In addition, during turn on, it also has a large current spike, a large di/dt and a high turn-on loss.

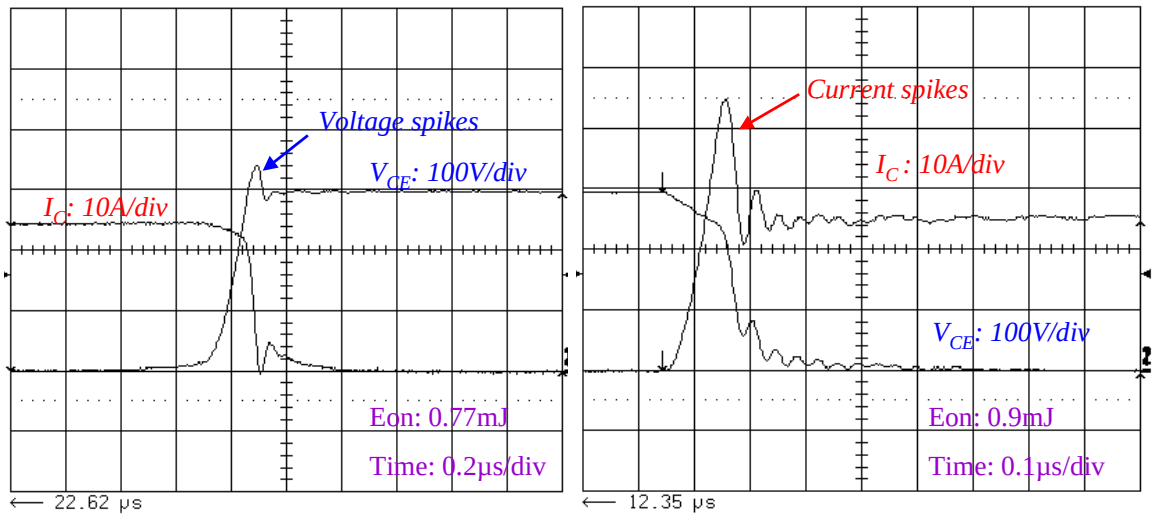

(a) Turn-off (b) Turn-on

Fig. A-10. Experimental IGBT switching voltage and current waveforms under hard-switching at 300-V bus and 25-A.

On the other hand, Fig. A-11 shows the current and voltage waveforms of the IGBT freewheeling diode under hard-switching conditions. As expected, diode reverse recovery of the anti-parallel diode affects the current stress of the switch in the opposite leg. This leads to overall poor efficiency and reliability for the converter.

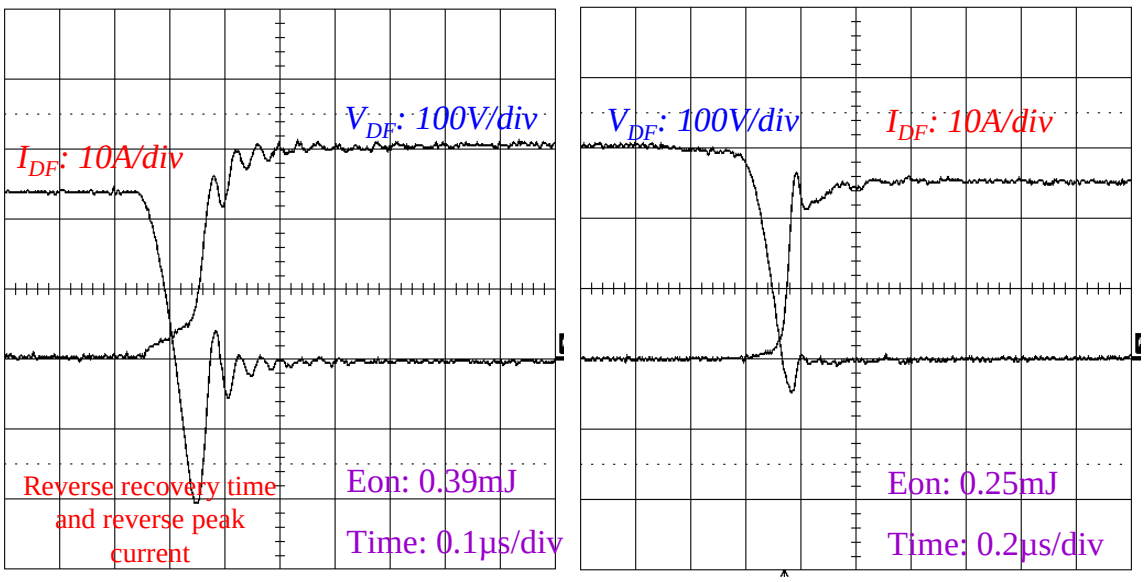

(a) Turn-off (b) Turn-on

Fig. A-11. Experimental IGBT free-wheeling diode switching voltage and current waveforms under hard-switching at 300-V bus and 25-A.

B. Soft-Switching

Voltage spike

Figures A-12(a) and (b) compare hard-switching (HS) and soft-switching (SS) converter device voltage spikes. With incorporation of SS, the voltage spike can be reduced by 46.7% from 375-V to 340-V as compared to HS. Typically, the voltage spike occurs because of parasitic

inductance. To reduce parasitic inductance, a laminated bus bar with larger surface area can be used.

EMI noises

Figures A-13 (a) and (b) show the turn-on EMI noise waveforms at a load current of 15-A. As shown in Fig. A-13(a), the traditional HS converter has turn-on EMI noises during turn-on because the IGBT current not only rises from zero to the load current immediately, but also adds a reverse recovery diode current. Thus, the current spikes occur with extremely high peak power consumption. In contrast, in the case of a soft-switching converter, the current spike never occurs because IGBT avoids the diode reverse recovery problem.

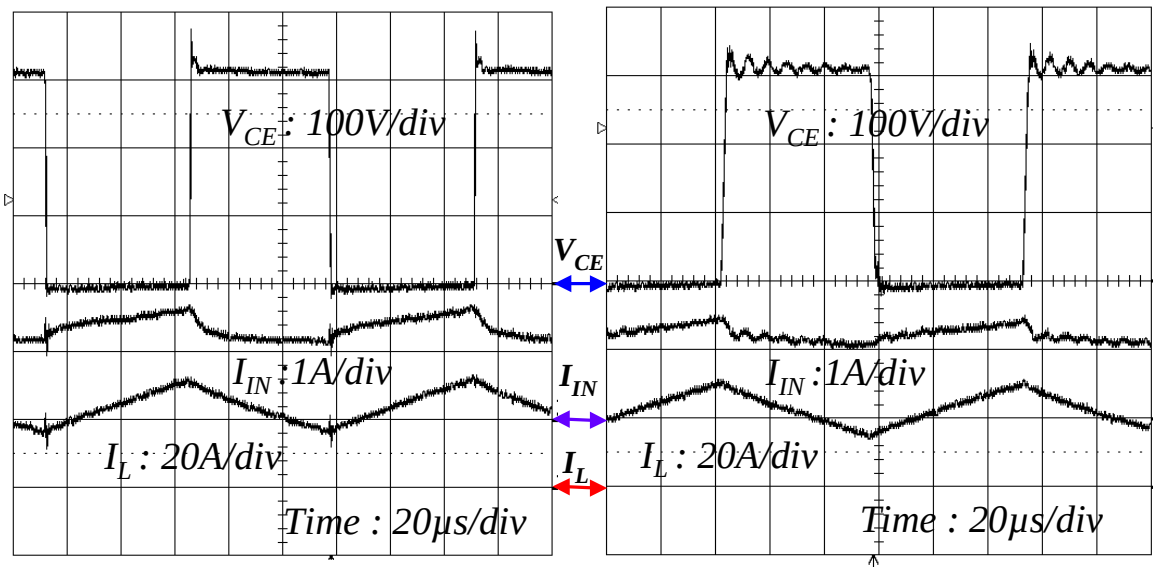

(a) Hard-switching chopper (b) Soft-switching chopper

Fig. A-12. Experimental current and voltage waveforms during turn-on and turn-off at a current of 25-A.

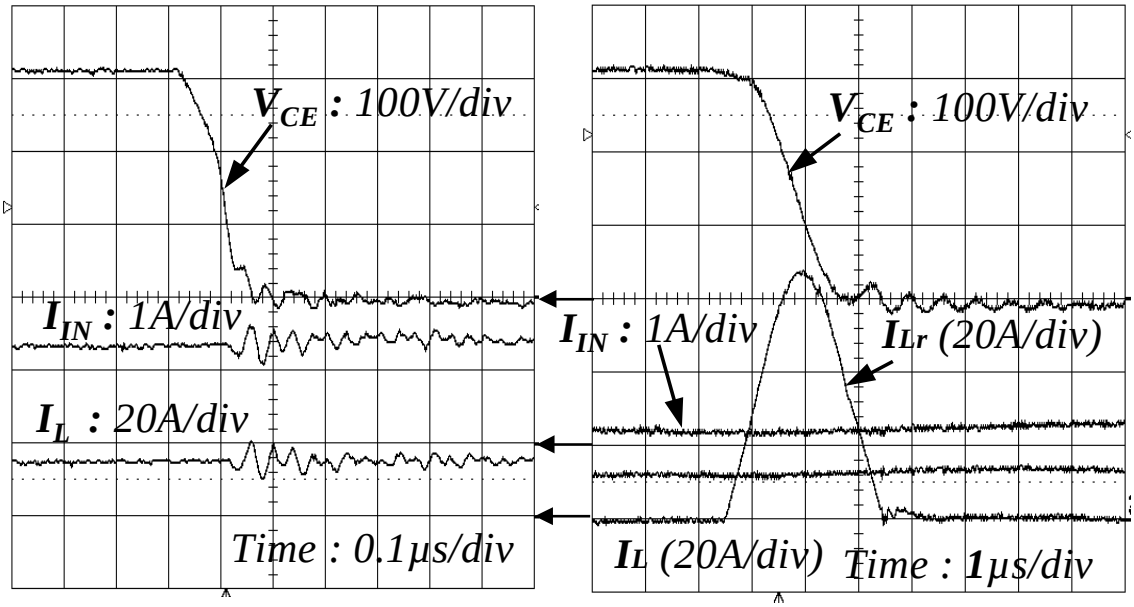

(a) Hard-switching converter (b) Soft-switching converter

Fig. A-13. Experimental current and voltage waveforms during turn-on.

Figures A-14 (a) and (b) compares the experimental HS and SS turn-off EMI noise waveforms at a load current of 30-A. As expected for hard-switching converters, during turn-off the device voltage rise with an overshoot due to the leakage inductance in the loop. Although this overshoot voltage can be reduced by a good circuit layout, the switch voltage-changing rate (dv/dt) can be extremely high, causing other associated problems such as a winding circulating current. Therefore, the developed soft-switching converter topology achieved the elimination of the EMI noises during both turn on and turn off.

Turn-off dv/dt

The turn-off dv/dt that was previously explained is shown in Fig. A-14. Fig. A-14(a) indicates that the turn-off dv/dt in the HS scheme was observed to be 2 kV/μs at a load current of 30 *A*. Fig. A-14(b) indicates that the turn-off dv/dt for the SS scheme was observed to be 110 V/μs at the same current. Compared to the previous results using only one capacitor as shown in

Fig. A-3(b), the dv/dt rate of the SS converter is replaced by one half because a capacitor with the same value is added across the free-wheeling diode. As a result, the turn-off dv/dt of the SS converter was 95% less than that of the HS converter.

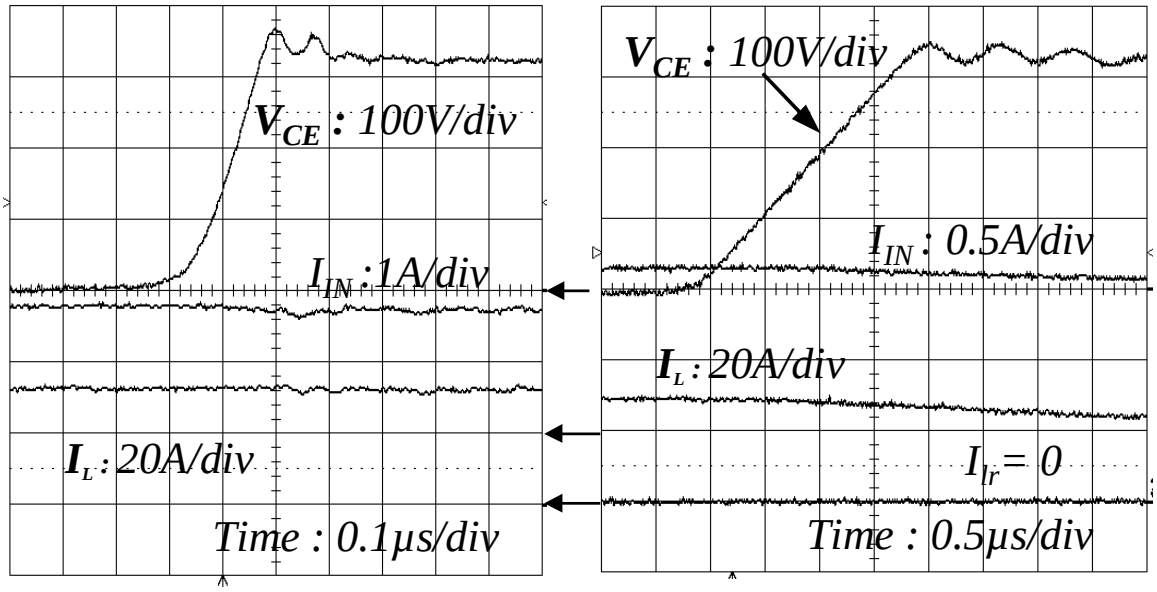

(a) Hard-switching converter (b) Soft-switching converter

Fig. A-14. Experimental voltage and current waveforms during turn-off.

Power loss

Using inductive load, the power loss can easily be measured as the difference between the input power and the I^2R loss in the load. As shown in Fig. A-15, the proposed TQSS converter achieves a total loss reduction of 30% and 34.6% at 25-A and 50-A, respectively. The experiment was performed with a switching frequency of 10 kHz. In the case of 20 kHz, the reduction of the power loss is expected be even more significant.

Heat sink temperature rise

With the converter loss reduction, it is expected that heat sink temperature can also be reduced. Fig. A-16 compares the rise in heat sink temperature between the hard- and soft-switching converters. The heat sink temperature of the proposed converter was reduced dramatically. The results indicate a 50% reduction of the heat sink temperature rise from 12℃ to 6℃ at 25-A, and from 31℃ to 15℃ at 50-A. Therefore, this means that the size of the heat sink can be cut by about 50%.

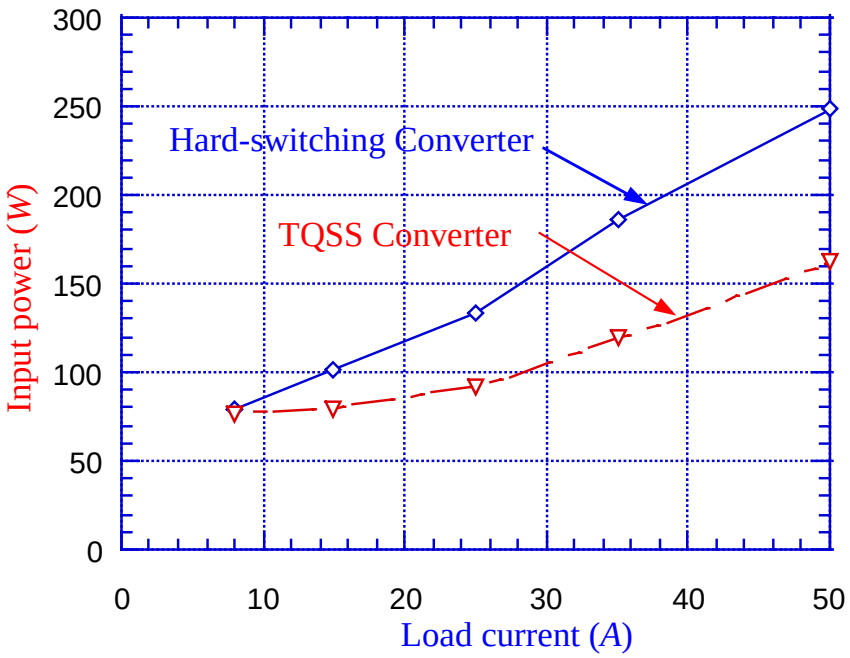

Fig. A-15. Input power comparison between hard-switching and soft-switching converters.

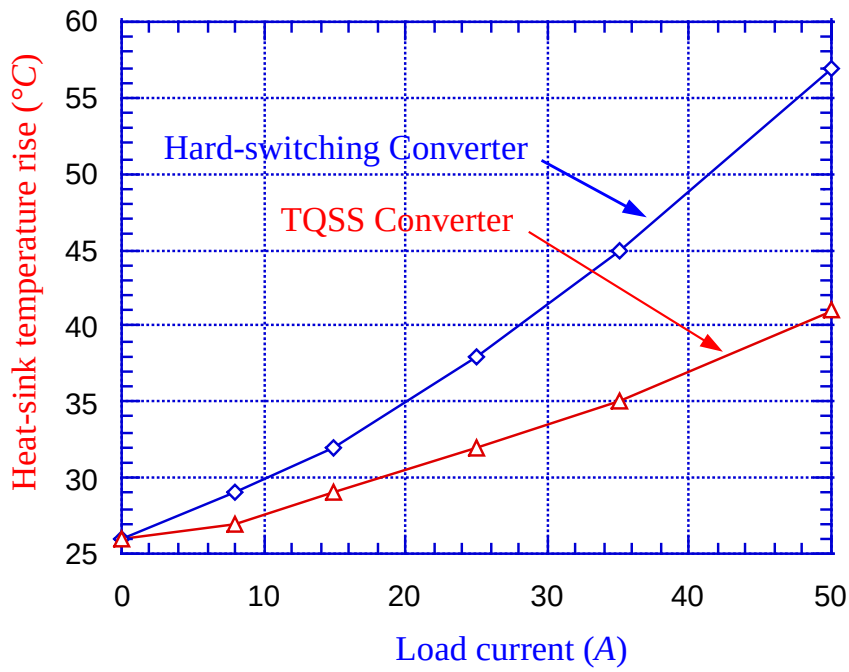

Fig. A-16. Heat sink temperature rise trajectories between hard-switching and soft-switching converters.

Control flexibility

To verify the loss of ZVT under inappropriate timing, an experiment was conducted under those conditions. Fig. A-17 shows the corresponding experimental result of the losing ZVT condition under incorrect timing. Voltage ringing was observed if the switch was turned on after the resonant current fell below the load current. This is because V_{CE} swings back to relatively higher voltage during that time. In this case, the reason that ZVT condition is lost is too much pre-charging time. So, we can achieve the zero-voltage condition by reducing the pre-charging time. Therefore, this converter requires that a proper pre-charging time be designed by considering the relationship between the load condition and the resonant tank.

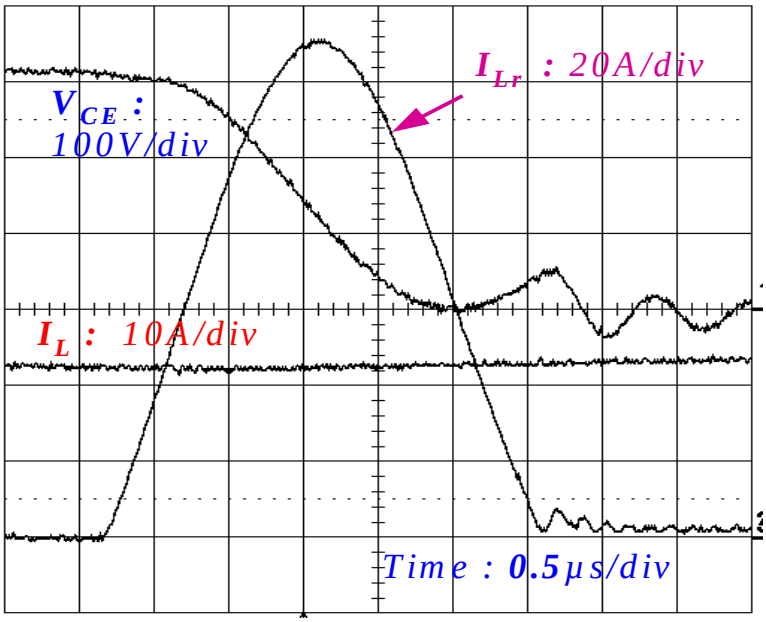

Fig. A-17. Switch voltage and current waveforms under incorrect timing.

Fig. A-18 shows the key waveforms of the load current I_L, the resonant current I_{Lr} and the voltage across the switch S_1 under different load current conditions. The timing design goal is to turn on the main switches at ZVT under the nominal operation condition of a load current of 25-A. Different load conditions are demonstrated such as the light load shown in Fig. A-18(a), the nominal load shown in Fig. A-18 (b), and the 50% overload shown in Fig. A-8 (c), respectively. The experimental results indicate that the proposed converter achieved the near-zero-voltage condition for wide variations in load current. This not only gives more control flexibility for the designer but also significantly reduces switching losses. In addition, the diode reverse recovery problem can also be avoided.

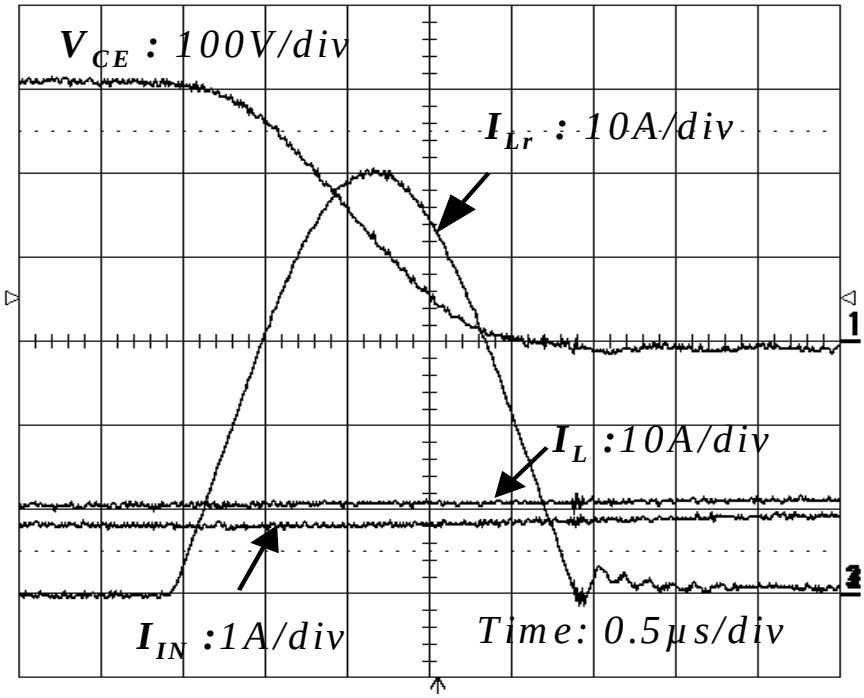
V_{CE} : 100V/div
I_{Lr} : 10A/div
I_L :10A/div
I_{IN} :1A/div
Time: 0.5μs/div

(a)

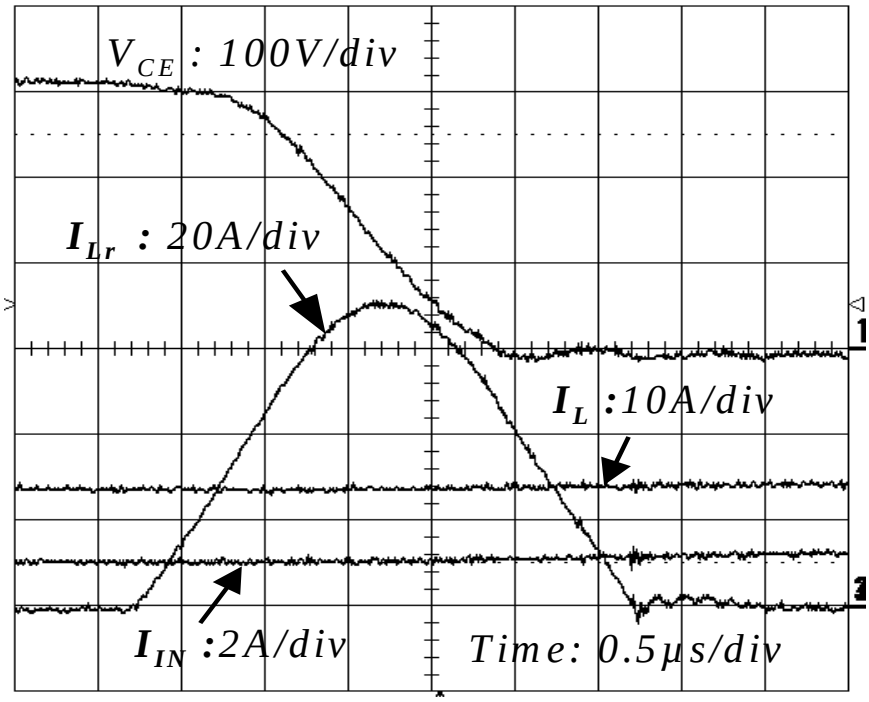
V_{CE} : 100V/div
I_{Lr} : 20A/div
I_L :10A/div
I_{IN} :2A/div
Time: 0.5μs/div

(b)

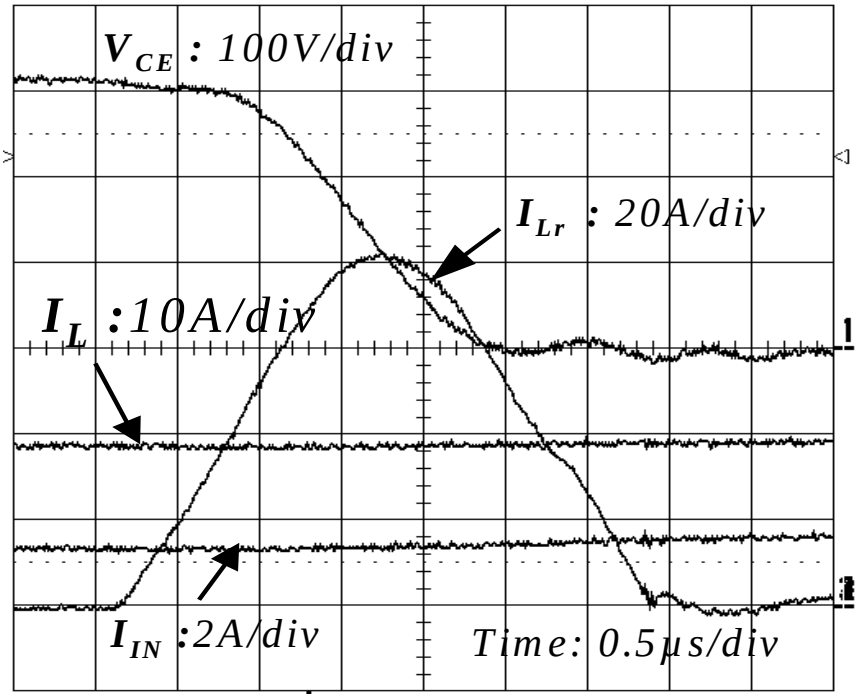

(c)

Fig. A-18. Resonant current and switch voltage waveforms under different load current conditions; (a) 11-A, (b) 28-A, and (c) 37-A.

A-V. CONCLUSION

In this section, a new soft-switching converter topology with a simple resonant snubber circuit was proposed and was verified fully for working conditions with an inductive load. In order to verify performance of the proposed converter, circuit simulations and experiments were conducted on a 15kVA IGBT converter. In conclusion, the proposed converter achieved: (1) total loss reduction by 30%, (2) *dv/dt* reduction from 2,000 to 110 V/μs, (3) voltage spike reduction from 375-V to 340-V, (4) lower turn-on noise, and (5) heat-sink temperature-rise reduction of 50%. The results show that the proposed converter not only saved weight and space but also reduced the cost of the converter while improving the performance.

REFERENCES

[1] J. S. Lai, R. W. Young, G. W. Ott, J. W. McKeever, and F. Z. Peng, "A Delta Configured Auxiliary Resonant Snubber Inverter," *IEEE Trans. on Ind. Appl.*, Vol. 32, No. 3, May/Jun. 1996, pp. 518–525.

[2] D. M. Divan, "The Resonant DC Link Converter -- A New Concept in Static Power Conversion," in *Conf. Rec. of IEEE-IAS*, Oct. 1986, pp. 648-656.

[3] W. McMurray, "Resonant Snubbers with Auxiliary Switches," *IEEE Trans. on Ind. Appl.*, Vol. 29, No. 2, Mar./Apr. 1993, pp. 355–362.2.

[4] H. Mao and F. C. Lee, "Improvement on Zero-Voltage Transition Three-Phase Rectifier/Inverter," in *Proc. of VPEC'95 Seminar*, Vol. 13, 1995, pp. 19-27.

[5] J. P. Gegner and C. Q. Lee, "Zero-Voltage Transition Converters using Inductor Feedback Technique," in *Conf. Rec. of IEEE-APEC*, Orlando, FL, Mar. 1994, pp. 862-868.

[6] R. W. De Doncker and J. P. Lyons, "The Auxiliary Resonant Commutated Pole Converters," in *Conf. Rec. of IEEE-IAS*, 1990, pp. 1228-1235.

[7] J. He and N. Mohan, " Parallel Resonant DC Link Circuit – A Novel Zero Switching Losses Topology with Minimum Voltage Stresses," in *Conf. Rec. of IEEE-PESC*, 1989, pp. 1006-1012.